## <u>Laser-assisted formation of 3c-SiC and continuous diamond growth using Si-Q carbon</u> on (100) silicon

Nayna Khosla<sup>1</sup>, Jagdish Narayan<sup>1</sup>\*, Roger Narayan<sup>2</sup>

- 1 Department of Materials Science and Engineering, Centennial Campus North Carolina State University, Raleigh, North Carolina 27695-7907, United States
- 2 Joint Department of Biomedical Engineering, Centennial Campus, North Carolina State University and UNC Chapel Hill, Raleigh, North Carolina 27695, United States

#### **Abstract**

The formation of 3c-SiC is of interest due to potential applications in the semiconductor industry; however, there are difficulties in obtaining 3c-SiC by conventional methods. Being a metastable phase, non-equilibrium growth conditions are favorable in the growth process. This paper reports the formation of nano-sized 3c-SiC by nanosecond laser annealing of Si-Q-carbon layers on the silicon (100), which is confirmed by its characteristic LO and TO peaks in the Raman spectra. We also show that the traditional HFCVD technique results in the 6H-polytype instead, as confirmed by SEM, Raman spectroscopy, and EBSD. Further, we investigate the role of these phases on the nucleation of heteroepitaxial diamond on a Si (100) substrate. We show that these phases as interlayers enhance the diamond growth significantly. The HRSTEM studies were performed to understand the interfacial structure and phase responsible for high diamond nucleation. These findings are significant for 3c-SiC and diamond electronics applications.

<sup>\*</sup> Corresponding author: J. Narayan (Email: j narayan@ncsu.edu)

### 1. Introduction

Silicon carbide (SiC) is a wide bandgap material; it has gained significant attention because of its utility in high-power devices and MEMS applications due to its high melting point and chemical inertness, which enable SiC devices to function in harsh high-power and high-temperature environments [1-4]. The SiC has also been used to nucleate diamond and form films on nondiamond substrates such as silicon [5,6]. Thermodynamically, SiC exists in different polytypes, which are differentiated by the stacking order of the tetrahedrally bonded Si-C bilayers. The cubic polytype of silicon carbide (3c-SiC) is obtained when the stacking is ABCABC..., which results in a pure zincblende structure [7]. While 3c-SiC is still an emerging semiconductor technology, 4H- and 6H- are the commercialized polytypes of SiC. The cubic polytype offers significant benefits over conventional hexagonal SiC polytypes. The 3c-SiC has a bandgap of 2.3eV; it is reported to show the highest channel mobility (>300 cm<sup>2</sup>/V/s) and saturation velocity ( $\sim 2 \times 10^7$ cms<sup>-1</sup>), which results in a considerable reduction in the power consumption of the devices [7]. Owing to its cubic symmetry, it shows isotropy in its properties. Also, 3c- is the only polytype that can be grown epitaxially on (100) Si wafers, which reduces the cost of using expensive SiC wafers. Therefore, the desired thickness of 3c-SiC can be grown on inexpensive Si wafers for the development of Si/SiC electronic devices. However, the yield of cubic polytype is very low due to a lack of device-quality substrates. Even from free energy considerations, it has been theoretically indicated that 6H and 4H polytypes possess lower free energy than 3c-SiC; thus, they are more stable [8].

Various methods have been used to grow 3c-SiC on Si substrates, such as evaporation, pulsed laser deposition, sputtering, chemical vapor deposition, and combustion synthesis [9-16]. In traditional CVD methods, the largest challenge to growing the cubic polytype is the metastability of this phase, in addition to the large lattice mismatch of ~20% and the thermal expansion coefficients of ~ 20% at 1200°C between 3c-SiC and Si. Most processing techniques use SiC as a template to form the cubic polytype because of an almost perfect lattice match between the 3c (111) and 6H/4H (0001) planes and the absence of a thermal expansion coefficient mismatch. However, the largest drawback is the large variations in the hexagonal polytype substrates and the narrow window of the growth parameters. Additionally, for growing 3c- via CVD, a temperature of ~1350°C or higher is required, which is close to the silicon melting temperature. This results in the mixture and redistribution of different precursor gas dopants on the Si substrate. No crystalline SiC growth was reported to be achieved below 1100°C [18,19]. In comparison with other methods, PECVD has the benefit of a low deposition temperature (200-300°C). It should be noted that SiC films made by PECVD are amorphous and contain considerable defects. Narayan et al. [8] reported a combustion synthesis method to form bulk 3c-SiC on Si using the diffusion of solid carbon into liquid silicon.

In this paper, we present an alternative processing approach to form thin film 3c-SiC directly on Si (100) using a non-equilibrium route based on liquid phase quenching of Si-Q carbon by excimer pulsed laser annealing (PLA); this is a highly desirable low-temperature processing technique due to its high annealing selectivity and steep temperature slope. We annealed silicon doped Q-carbon layer deposited on Si (100); this process results in melting and quenching of silicon, leading to the formation of cubic polytype. We also show that there is a preferential growth of 6H-SiC on (100) Si by the hot filament CVD technique.

We further investigated the use of 3c-SiC to provide nucleation sites for diamond film growth. The CVD diamond films have high thermal conductivity, high insulation, and a large reverse breakdown field, which make them a suitable candidate for heat dissipation applications, especially in high-power devices [21,22]. However, depositing diamond films on non-diamond substrates is impeded by a lower nucleation density due to a lack of covalent bonding combined with a high surface energy. Therefore, non-diamond substrates (e.g., Si) are seeded with diamond nanoparticles, resulting in the requirements of external seeding and impurity contamination. On carbide-forming substrates, it has been suggested that the creation of a carbide layer is a prerequisite for diamond nucleation and growth. The formation of carbide layers lowers surface energy ( $\gamma$ ) and hence the critical size of nuclei  $r^*$  (=2  $\gamma$ /  $\Delta G$ ), where  $\Delta G$  is the free energy of the diamond phase. Thus, SiC is somewhat effective in diamond nucleation. However, Q-carbon is most effective since it consists of a high density of diamond tetrahedra that are packed together. The utility of Q-carbon in supplying nucleation sites for diamond growth has been reported by Narayan et al. [23] In this paper, we perform a comparative study and show the evidence of some enhancement of diamond growth by SiC on Si using the hot-filament CVD technique and highlight the superiority of a Q-carbon layer over a silicon carbide layer as a better template to form a highly dense and continuous diamond film on silicon.

In this paper, we show that non-equilibrium ultrafast laser processing is suitable to form 3c-SiC by annealing Si-doped Q-carbon on a (100) Si wafer, whereas the hexagonal polytype of SiC on (100) silicon is formed by HFCVD processing [24]. We also report the formation of large-area, faceted diamond films on Si-Q and 3c-SiC interlayer by HFCVD; in addition, we show the supremacy of Q-carbon over SiC to nucleate continuous, stress-free diamond films.

### 2. Results and discussion

#### 2.1. Pulsed laser annealing of Si-Q to form 3c-SiC

We deposited a 10 nm thick Si-Q carbon layer on a high resistivity Si substrate by PECVD, as proposed by Narayan et al. [25]. The formation of the Q-layer is associated with the presence of a signature Q-carbon peak in Raman spectra, as will be shown later. These samples were then laser annealed using an ArF laser at 0.6-0.8 Jcm<sup>-2</sup> energy density with 20 ns pulse duration, which is

suitable to anneal the Si-Q carbon without ablation. It was observed that annealing results in the formation of nano 3c-SiC agglomerates, as shown in Fig.1. During PLA by a 25 ns pulse width, 193 nm ArF laser at this energy density raises the temperature up to 2000°C for nanoseconds, which is much higher than the temperature at which the Si-DLC films remain thermally stable. It is envisaged that the Si-Q layer and tens of nanometers of silicon substrate melt; carbon diffuses rapidly into the liquid silicon, involving liquid phase diffusion. This layer is quenched to form nano-sized 3c-SiC, as shown in the inset of Fig.1. The diffusion coefficient of carbon in liquid silicon is ~10<sup>-4</sup>cm<sup>2</sup>/s, and the overall reaction is favorable with negative Gibbs free energy [8,26]. The boundary and nearby areas show carbonization of Q-carbon, which provides nanodiamond nucleation sites. Since the energy density follows a Gaussian profile, the energy transferred at these sites is not enough to reach the lattice of the Si substrate and cause melting.

The bonding characteristics of the film were further confirmed by Raman spectroscopy; it is a powerful technique to identify the SiC polytype at ambient temperature [27]. The spectra were recorded by focusing the laser beam on the 3c-SiC regions marked in blue and on the boundaries of these regions. The Raman spectra of Si-Q are considered as a reference to analyze the changes post-annealing, as shown in Fig. 1b. A sharp peak at 520 cm<sup>-1</sup> corresponds to the first-order scattering of the crystalline Si substrate. The Si-Q spectra show a signature Q-carbon peak between 1335 cm<sup>-1</sup> and 1576 cm<sup>-1</sup>, along with 520 cm<sup>-1</sup> (not shown in this scale). The 730 cm<sup>-1</sup> and 945 cm<sup>-1</sup> peaks arise due to Si-Si interaction from the dopant Si and the substrate [25,28]. The peak from the Si substrate is seen because the penetration depth for the excitation wavelength (532 nm) exceeds the film thickness. The 3c-SiC spectrum is obtained in regions marked with blue. The Si-C bonds are associated with a band that is located in the region between 700 and 1000 cm<sup>-1</sup> [29]: it is seen to enhance after post-annealing from the marked regions as shown in Fig. 1b, confirming the formation of SiC polytype [30]. The simplest polytype associated with the shortest period is the 3c polytype, which exhibits a zincblende (cubic) structure. Group theory analysis indicates that a number of phonon modes occur at the  $\Gamma$  point for higher polytypes that correspond to the folded modes since their unit cell contains a number of atoms. The unit cell of 3c-SiC exhibits one formula unit; a LO mode and doubly degenerate TO modes are noted in the optical branches [31]. The cubic polytype (3c-SiC) exhibits only two optical modes at  $\Gamma$  that are Raman active: the transverse one (TO) at 799 cm<sup>-1</sup> and the longitudinal one (LO) at 977 cm<sup>-1</sup> [32]. In this case, we observe a prominent sharp peak at 775 cm<sup>-1</sup>; the LO peak is overlapped with the second-order Raman spectrum of silicon that is noted between 930 cm<sup>-1</sup> and 1050 cm<sup>-1</sup>. No other peak associated with the other polytype of SiC is seen, which confirms the formation of 3c-SiC. The downshift in the peak is attributed to the formation of nano-sized 3c-SiC and quantum confinement effects [33]. The strong D-peak at 1330 cm<sup>-1</sup> and G-peak at 1576 cm<sup>-1</sup> are associated with the amorphous sp<sup>2</sup> carbon that is seen at the grain boundaries circumscribing the SiC region, indicating the existence of quenched carbon phase and nanodiamonds [22,23]. The G-peak is associated with the E2g mode at the  $\Gamma$ -point, and arises from the stretching of the C-C bond; this finding is common to all sp<sup>2</sup>hybridized carbon systems. The presence of disorder in sp<sup>2</sup>-hybridized carbon is associated with

the D-peak. However, these peaks are reduced significantly in the 3c-SiC confined regions, showing the presence of only the 3c-SiC phase.

### 2.2. HFCVD of Si-Q carbon film to form 6H SiC

Si-Q carbon layered silicon (100) sample was treated using hot filament chemical vapor deposition (HFCVD) for 3 hours. We observed the formation of the hexagonal polytype of SiC in the form of plates with stacked overgrowth on it. Fig. 2a shows an SEM image of the films grown on the Si-Q/Si substrate. Growth steps were noted on the film grown on the Si substrate at a tilt of 30 degrees with respect to the substrate. These as-grown surfaces of the films were noted to be very flat, smooth, and shiny. The 6H-SiC plate formations were confirmed by Raman spectroscopy as shown in Fig. 2b. The sharp peaks at 666 cm<sup>-1</sup>, 819 cm<sup>-1</sup>, and 995 cm<sup>-1</sup> characterize the 6H-SiC phase formed post-HFCVD. The undoped 6H-SiC is characterized by the TO peak (801 cm<sup>-1</sup>) and the LO peak (970 cm<sup>-1</sup>) [34]. The EBSD Kikuchi pattern data shown in Figs. 2(c and d) were obtained on the silicon site and the plate site, respectively. This result further confirms the formation of hexagonal SiC and establishes the epitaxial ordering of these 6H-SiC plates with respect to the Si substrate. These results show that the Si-Q carbon interlayer can facilitate the growth of epitaxial 6H-SiC directly on Si.

### 2.3. Characterization of diamond films by HFCVD

These annealed films were used for diamond deposition by HFCVD for 3 hours without diamond seeding. The SEM images in Fig. 3 show that well-faceted diamonds with preferential growth orientations are formed in the annealed samples, indicating the high crystalline quality of the films; this finding will also be confirmed by the Raman spectra later. The diamond film morphology is related to the preferential growth of different planes along different directions. When the growth rate along the [100] direction is the highest, the resultant morphology is octahedron crystals, which are surrounded by (111) planes. As such, the intermediate growth rates are associated with cubooctahedron crystals [35]. In our case, we see octahedron morphology. It is interesting to note that the diamonds on these films are highly dense compared to the ones grown on Si substrate (Fig. S2), suggesting that 3c-SiC and Q-carbon provide high nucleation sites for diamond growth. In fact, diamond nucleation in Q-carbon has no free-energy barrier as the diamond tetrahedra are already there. The nucleation on 3c-SiC is lower than on Q-carbon but higher than on Si. This finding is because of the sp<sup>3</sup> bonding of Si-C bonds, which lowers the surface energy  $(\gamma)$  and hence the critical size of diamond nuclei ( $r^* = 2 \frac{\gamma}{\Lambda G}$ ). Fig. 3(a) shows diamond nucleation in the regions with the SiC interlayer. It can be noted that the (100) planes are surrounded by (111) planes forming the diamond. Fig. 3(b) shows diamond nucleation on the Si-Q carbon. It is interesting to note that the nucleation on this Q-carbon layer is much higher than on 3c-SiC sites. The diamond film is discontinuous on 3c-SiC compared to the continuous diamond film provided by the Qcarbon interlayer. The (111) facets of the diamond pyramids were visible.

The crystallinity of the diamonds and film sites was further confirmed by Raman spectroscopy, as shown in Fig.4. Fig. 4(a) shows Raman spectra taken from the SiC site, which nucleated discontinuous diamonds. These peaks are similar to Raman spectra peaks shown above, confirming the presence of SiC on this site. The diamond on this site shows a sharp peak at 1333.5 cm<sup>-1</sup>, as shown in Fig. (b). The peak shift of 1.5cm<sup>-1</sup> indicates stress in the film due to the difference in their thermal expansion coefficients, creating a thermal misfit strain at the interface. Fig. 4 (c) shows the Raman spectrum at the site of continuous diamond film. High nanodiamond nucleation post-annealing by Q-carbon interlayer at this site resulted in faceted highly dense diamond growth. The spectrum at this site shows no peaks of any polytype of SiC, confirming that there is no SiC. The diamond spectrum from this site, as shown in Fig. 4 (d), shows the diamond peak at 1332.3cm<sup>-1</sup>, further confirming the crystalline quality of fully relaxed diamond film.

To understand the structural characteristics, epitaxy, and role of the Q-carbon interlayer, we performed STEM/TEM cross-sectional studies. The STEM images in Fig.5 show that there is a very thin interlayer on Si substrate comprised of Q-carbon, which aids the nucleation of diamond. No diamond is formed directly on the Si substrate. Fig. 5 (a) shows individual columns of diamond crystallites with a thin layer of Q-carbon, which is clearly shown in the high-resolution micrograph in Fig. 5 (b), as an interlayer consisting of amorphous Q-carbon. The STEM image of diamond in Fig. 5(c) shows a columnar growth structure of the diamonds. Distinct, individual crystallites exhibiting textured orientations were observed; the columns begin to grow over the randomly oriented crystallites after they coalesce with one another. Vertical direction growth takes place along the fastest-growing planes that are prevalent in the crystals; the resulting as-grown surface exhibits a very high surface roughness because of the difference in heights associated with the growing columns. The <110> electron diffraction pattern from diamond and silicon is shown in Fig. 5(d).

The role of Q-carbon in diamond nucleation is delineated clearly from chemical mapping and EELS studies, as shown in Fig 6(a) and 6(b), respectively. The intensity of Si is the brightest in the substrate as expected; it decreases in the interlayer and to zero in the diamond region. Conversely, the diamond region shows the highest intensity in carbon mapping, which decreases significantly in the interlayer and is completely absent in the substrate area. This finding shows that the interlayer (~5nm thickness) essentially consists of Si and C elements. From the oxygen mapping, we observe the presence of some oxygen at this interlayer as well. This finding indicates the presence of some native oxide, SiOx. The native oxide layer is a very thin (approx. <1.5nm) layer of SiO<sub>x</sub> that forms on the surface of a silicon wafer on exposure to air. The carbon content is from the Q-carbon layer. Therefore, Q-carbon layer is not directly connected with the Si substrate but rather on top of the native amorphous SiOx layer, which results in the absence of an epitaxial relationship. In order to understand the bonding characteristics, EELS studies were conducted with an aberration-corrected STEM-FEI Titan 80-300 that provides an energy resolution of 0.15 eV. EELS spectra at the interlayer show the Q-carbon presence marked by Q-carbon exhibits a sloping

edge at 287 eV [36] with a broad peak at 291 eV corresponding to  $\pi^*$  and  $\sigma^*$  edges, respectively. The diamond EELS show a signature spectrum that includes a sharp edge at 290 eV with a peak at 292 eV, which corresponds to sp<sup>3</sup> ( $\sigma^*$ ) bonding; in silicon, no such peaks are observed as expected.

It is envisaged that HFCVD leads to the formation of thermally stable 6H-SiC, as confirmed by the Raman spectroscopy. Once this interlayer reaches the desired thickness, silicon diffusion slows for further growth, and diamond nucleation is followed. SiC growth always precedes diamond nucleation. The diamond grown on 6H-SiC is dense but discontinuous compared to the one grown with a Q-carbon interlayer. This finding shows that Q-carbon aided the growth of nanodiamonds, which provided higher nucleation density than the 3c-SiC phase. However, in our case, the presence of a native oxide layer, which was formed during the initial deposition of the Si-Q carbon layer that suppressed the epitaxy. It is surmised that if this layer is removed prior to the deposition, we can get not only a large area and continuous faceted diamond growth but also epitaxial diamond film using Si-Q interlayer.

#### 3. Conclusions

We report the growth of two distinct phases of SiC by two different techniques using a Si-Q carbon layer on a Si substrate. We successfully show the role of pulsed laser annealing, a non-equilibrium technique to form nano-sized 3c-SiC and nanodiamonds using Si-Q layers on the silicon (100) wafer. The crystalline phase of 3c-SiC is confirmed by the signature LO and TO peaks observed in Raman spectra. We used hot filament chemical vapor deposition to directly grow 6H-SiC films on Si (100). This finding is confirmed by SEM, Raman spectroscopy, and EBSD. The formation of cubic polytope of SiC is highly advantageous for solid state devices. Also, the growth of 3c-SiC directly on the Si substrate helps negate the need for an expensive SiC substrate. Wafer-scale integration of Si-doped Q-carbon opens the possibility of a high level of scalability for this process. We also have used these phases of 3c-SiC and Q-carbon/nanodiamonds as interlayers to show the superiority of these phases to nucleate diamond compared to bare silicon by the hot filament CVD process. SEM images confirm the formation of large-area faceted diamond film at 3c-SiC and Q-Carbon sites. Octahedron diamonds growing in [100] direction, surrounded by (111) planes, are observed. However, the nucleation on 3c-SiC is lower than Q-carbon but higher than on Si. This finding is because of the sp<sup>3</sup> bonding of Si-C bonds, which lowers the surface energy  $(\gamma)$  and hence the critical size of diamond nuclei. The higher nucleation density over a large area with Q-carbon interlayer shows that Si-Q interlayer provides higher nucleation sites than the carbide layer. These interesting results are further confirmed by the Raman spectroscopy data. The Raman spectra show crystalline and high-quality diamond films. A little upshift of 1.5cm<sup>-1</sup> is observed in the carbide interlayer spectrum, indicating some stress. However, diamond films are very much stress-free and phase-pure on Q-carbon interlayer. To understand such high nucleation growth, HRTEM studies were performed, which suggested the superiority of Si-Q carbon interlayer to nucleate nanodiamond sites post-annealing. These sites resulted in effectively dense and faceted octahedral

diamond films. The presence of a native oxide layer impeded the epitaxial relationship. However, if this layer is removed before Si-Q deposition, then we can get stress-free large-area epitaxial diamond films on suitable substrates for high-power, high-temperature devices.

### 4. Experimental Procedure

We used 10nm thick Si doped Q-carbon films deposited on (100) silicon substrate using the plasma enhanced chemical vapor deposition (PECVD) approach, as reported by Narayan et al. [24], as our reference samples. The custom-designed PECVD instrument produces plasma in the capacitively coupled mode. The deposition procedure involves several steps, including a loading step, plasma cleaning step, plasma deposition step, post-processing step, and unloading step. Once  $\sim 2x10^{-8}$  Torr pressure was reached, plasma cleaning was performed for 10 min with argon gas at a mass flow rate of 90 SCCM. The deposition was undertaken using 1.6 SCCM of trimethylsilane (TMS) and 90 SCCM of argon for 3 minutes. The peak-to-peak voltage (Vpp) during this process was kept at 300  $\pm 10$  V using an RF power of 83  $\pm$  10 W and a DC bias of -150  $\pm$  10 V. This was followed by post-processing with 90 SCCM argon gas at an RF power of 160  $\pm 10$  W, a Vpp of 500  $\pm$  10 V, and a DC bias of 250  $\pm$  10 V over 5 minutes. During the steps, the total pressure was maintained at 50m Torr using a MKS Baratron gauge.

The as-deposited Si-Q carbon samples were annealed with ArF excimer laser pulses having a wavelength of 193 nm, pulse duration of 25 ns, photon energy of 6.4 eV, and energy density varying from 0.6 Jcm<sup>-2</sup> to 0.8 Jcm<sup>-2</sup>. The annealing energy density was controlled with the focusing lens. ArF excimer lasers exhibit a higher absorption coefficient and a smaller penetration depth profile, which leads to increased temperature differences between the film and the substrate. The laser-treated films were evaluated using high-resolution SEM and Raman spectroscopy to investigate the evolution of microstructures after annealing.

Faceted diamond growth on these samples were carried out using the hot filament chemical vapor deposition (HFCVD) technique. During this process, four tungsten filaments were used. A  $9 \pm 0.1$  V voltage and  $90 \pm 10$  A current were applied to raise the filament temperature ~2000 °C. The samples were kept on the substrate holder whose temperature was raised to  $800 \pm 25$  °C. The substrate holder was kept at about 5 mm below these filaments. Samples were carburized for 7 min using a flow rate of 50 standard cubic centimeter per minute (sccm) for CH<sub>4</sub>, and 10 sccm for H<sub>2</sub> gas at a chamber pressure of 10 Torr. During the carburization process, the substrate was placed away from the hot filament. The CVD growth took place under a flow rate of 2 sccm for CH<sub>4</sub> and 100 sccm for H<sub>2</sub> using a chamber pressure of 20 Torr for 3 hours. The gas flow rates were measured with mass flow controllers (MKS Instruments, Inc., Andover, MA). After the deposition process, the substrate was cooled using a constant cooling rate of 10 °C/min in order to minimize the thermal shock effect. The HFCVD samples were characterized by HRSEM, EBSD, Raman spectroscopy, HRSTEM, and EELS. High-resolution SEM imaging with sub-nanometer resolution was conducted using a FEI Verios 460L SEM (Hillsboro, OR, USA) with an EBSD attachment. The WITec confocal Raman microscope system (532 nm laser source) (Ulm, Germany) containing

a grating size of 1800 I/mm was used to study the Raman-active vibrational modes. Crystalline Si was utilized to calibrate the Raman spectra since it is associated with a characteristic Raman peak at 520.6 cm<sup>-1</sup>. A FEI Quanta 3D FEG dual beam instrument (Hillsboro, OR, USA) containing both electron and ion beam guns was used to create cross-sectional TEM samples. A low-energy ion beam (5 kV, 10 pA) was utilized to treat the focused ion beam (FIB) surface damage. An aberration-corrected FEI STEM Titan 80-300 instrument (Hillsboro, OR, USA) was used in conjunction with EELS (with a resolution of 0.15 eV) to obtain high angle annular dark field (HAADF) images and EELS spectra from the diamond thin films. The electron probe current used in this study was  $38 \pm 2$  pA. The EELS data were obtained using a collection angle of 28 mrads.

#### 5. Acknowledgments

This work was supported by the National Science Foundation Grant 1836767 and 2016256. We are thankful to Dr. Parand Riley for the Si-Q reference samples. The comments and discussions with Professor John Prater are gratefully acknowledged. This work was performed in part at the Analytical Instrumentation Facility (AIF) at North Carolina State University, which is supported by the State of North Carolina and the National Science Foundation (award number ECCS-2025064). The AIF is a member of the North Carolina Research Triangle Nanotechnology Network (RTNN), a site in the National Nanotechnology Coordinated Infrastructure (NNCI).

#### **Data Availability Statement**

The datasets used and/or analyzed during the current study will be available from the corresponding author upon reasonable request.

### 6. References

- [1] Sarro, P. M. (2000). Silicon carbide as a new MEMS technology. Sensors and Actuators A: Physical, 82(1-3), 210-218.
- [2] Zhao, J. H., Pensl, G., Kimoto, T., Matsunami, H., Kosugi, H., Cooper, J. A., & Weiner, M. (2008). Special issue on silicon carbide devices and technology. IEEE Transactions on Electron Devices, 55(8), 1795-1797.
- [3] Mehregany, M., Zorman, C. A., Rajan, N., & Wu, C. H. (1998). Silicon carbide MEMS for harsh environments. Proceedings of the IEEE, 86(8), 1594-1609.
- [4] Arbiol, J., & Xiong, Q. (Eds.). (2015). Semiconductor nanowires: materials, synthesis, characterization and applications. Elsevier.
- [5] Jiang, X., & Klages, C. P. (1996). Recent developments in heteroepitaxial nucleation and growth of diamond on silicon. physica status solidi (a), 154(1), 175-183.
- [6] Gogotsi, Y., Welz, S., Ersoy, D. A., & McNallan, M. J. (2001). Conversion of silicon carbide to crystalline diamond-structured carbon at ambient pressure. *Nature*, 411(6835), 283-287.
- [7] La Via, F., Severino, A., Anzalone, R., Bongiorno, C., Litrico, G., Mauceri, M., ... & Wellmann, P. (2018). From thin film to bulk 3C-SiC growth: Understanding the mechanism of defects reduction. Materials Science in Semiconductor Processing, 78, 57-68.

- [8] Narayan, J., Raghunathan, R., Chowdhury, R., & Jagannadham, K. (1994). Mechanism of combustion synthesis of silicon carbide. Journal of applied physics, 75(11), 7252-7257.
- [9] Laref, A., & Laref, S. (2008). Electronic and optical properties of SiC polytypes using a transferable semi-empirical tight-binding model. physica status solidi (b), 245(1), 89-100.
- [10] Tairov, Y. M., Tsvetkov, V. F., Lilov, S. K., & Safaraliev, G. K. (1976). Studies of growth kinetics and polytypism of silicon carbide epitaxial layers grown from the vapour phase. Journal of Crystal Growth, 36(1), 147-151.
- [11] Boo, J. H., Lee, S. B., Yu, K. S., Sung, M. M., & Kim, Y. (2000). High vacuum chemical vapor deposition of cubic SiC thin films on Si (001) substrates using single source precursor. Surface and Coatings Technology, 131(1-3), 147-152.
- [12] Barbouche, M., Benabderrahmane Zaghouani, R., Benammar, N. E., Khirouni, K., & Ezzaouia, H. (2017). Synthesis and characterization of 3C-SiC by rapid silica carbothermal reduction. The International Journal of Advanced Manufacturing Technology, 91(1), 1339-1345.
- [13] Dong, Y., Zorman, C., & Molian, P. (2003). Femtosecond pulsed laser micromachining of single crystalline 3C–SiC structures based on a laser-induced defect-activation process. Journal of Micromechanics and Microengineering, 13(5), 680.
- [14] Steckl, A. J., Yuan, C., Li, J. P., & Loboda, M. J. (1993). Growth of crystalline 3C-SiC on Si at reduced temperatures by chemical vapor deposition from silacyclobutane. Applied physics letters, 63(24), 3347-3349.
- [15] Itoh, H., Yoshikawa, M., Nashiyama, I., Misawa, S., Okumura, H., & Yoshida, S. (1990). Radiation induced defects in CVD-grown 3C-SiC. IEEE Transactions on nuclear science, 37(6), 1732-1738.
- [16] Zhuang, H., Zhang, L., Staedler, T., & Jiang, X. (2013). Low temperature hetero-epitaxial growth of 3C-SiC films on Si utilizing microwave plasma CVD. Chemical Vapor Deposition, 19(1-3), 29-37.
- [17] Gupta, A., & Jacob, C. (2005). Selective epitaxy and lateral overgrowth of 3C-SiC on Si–A review. Progress in crystal growth and characterization of materials, 51(1-3), 43-69.
- [18] Yoshinobu, T., Nakayama, M., Shiomi, H., Fuyuki, T., & Matsunami, H. (1990). Atomic level control in gas source MBE growth of cubic SiC. Journal of crystal growth, 99(1-4), 520-524.
- [19] Wang, L., Dimitrijev, S., Han, J., Iacopi, A., Hold, L., Tanner, P., & Harrison, H. B. (2011). Growth of 3C–SiC on 150-mm Si (100) substrates by alternating supply epitaxy at 1000 C. Thin solid films, 519(19), 6443-6446.
- [20] Iliescu, C., & Poenar, D. P. (2012). PECVD amorphous silicon carbide (α-SiC) layers for MEMS applications. In Physics and Technology of Silicon Carbide Devices. IntechOpen.
- [21] Graebner, J. E., Jin, S. K., & GW, H. (1992). JA and Gardinier, CF Appl. Phys. Lett, 60, 1576.
- [22] Okushi, H. (2001). High quality homoepitaxial CVD diamond for electronic devices. Diamond and Related Materials, 10(3-7), 281-288.

- [23] Khosla, N., & Narayan, J. (2022). Fabrication of Q-Carbon Nanostructures, Diamond and Their Composites with Wafer-Scale Integration. Crystals, 12(5), 615.
- [24] Khosla, N. Laser Processing of Q-Carbon, Diamond, and Anode and Cathode for Lithium-Ion Batteries. North Carolina State University; 2023.
- [25] Riley, P. R., Joshi, P., Khosla, N., Narayan, R. J., & Narayan, J. (2022). Formation of Q-carbon with wafer scale integration. Carbon. Volume 196,2022, Pages 972-978, ISSN 0008-6223.
- [26] Luo, J., Alateeqi, A., Liu, L., & Sinno, T. (2017). Atomistic simulations of carbon diffusion and segregation in liquid silicon. Journal of Applied Physics, 122(22), 225705.
- [27] Okumura, H., Sakuma, E., Lee, J. H., Mukaida, H., Misawa, S., Endo, K., & Yoshida, S. (1987). Raman scattering of SiC: Application to the identification of heteroepitaxy of SiC polytypes. Journal of applied physics, 61(3), 1134-1136.
- [28] Narayan, J., & Khosla, N. (2022). Self-organization of amorphous Q-carbon and Q-BN nanoballs.
- [29] Inoue, Y., Nakashima, S., Mitsuishi, A., Tabata, S., & Tsuboi, S. (1983). Raman spectra of amorphous SiC. Solid state communications, 48(12), 1071-1075.
- [30] Zgheib, C., McNeil, L. E., Kazan, M., Masri, P., Morales, F. M., Ambacher, O., & Pezoldt, J. (2005). Raman studies of Ge-promoted stress modulation in 3C–SiC grown on Si (111). Applied Physics Letters, 87(4).
- [31] Nakashima, S. I., & Harima, H. (1997). Raman investigation of SiC polytypes. physica status solidi (a), 162(1), 39-64.
- [32] Zhuravlev, K. K., Goncharov, A. F., Tkachev, S. N., Dera, P., & Prakapenka, V. B. (2013). Vibrational, elastic, and structural properties of cubic silicon carbide under pressure up to 75 GPa: Implication for a primary pressure scale. Journal of Applied Physics, 113(11), 113503.
- [33] Bechelany, M., Brioude, A., Cornu, D., Ferro, G., & Miele, P. (2007). A Raman spectroscopy study of individual SiC nanowires. Advanced Functional Materials, 17(6), 939-943.
- [34] Bauer, M., Gigler, A. M., Huber, A. J., Hillenbrand, R., & Stark, R. W. (2009). Temperature-depending Raman line-shift of silicon carbide. Journal of Raman Spectroscopy: An International Journal for Original Work in all Aspects of Raman Spectroscopy, Including Higher Order Processes, and also Brillouin and Rayleigh Scattering, 40(12), 1867-1874.
- [35] Mallik, A. K., Dandapat, N., Chakraborty, S., Mandal, A. K., Ghosh, J., Unnikrishnan, M., ... & Balla, V. K. (2014). Characterizations of microwave plasma CVD grown polycrystalline diamond coatings for advanced technological applications. Processing And Application Of Ceramics, 8(2), 69-80.
- [36] Narayan, J., & Bhaumik, A. (2016). Q-carbon discovery and formation of single-crystal diamond nano-and microneedles and thin films. Materials Research Letters, 4(2), 118-126.

### **Authors Contributions**

Nayna Khosla: Investigation, Methodology, Data curation, Writing- Original draft preparation, Writing- Reviewing and Editing, Writing- Reviewing and Editing.

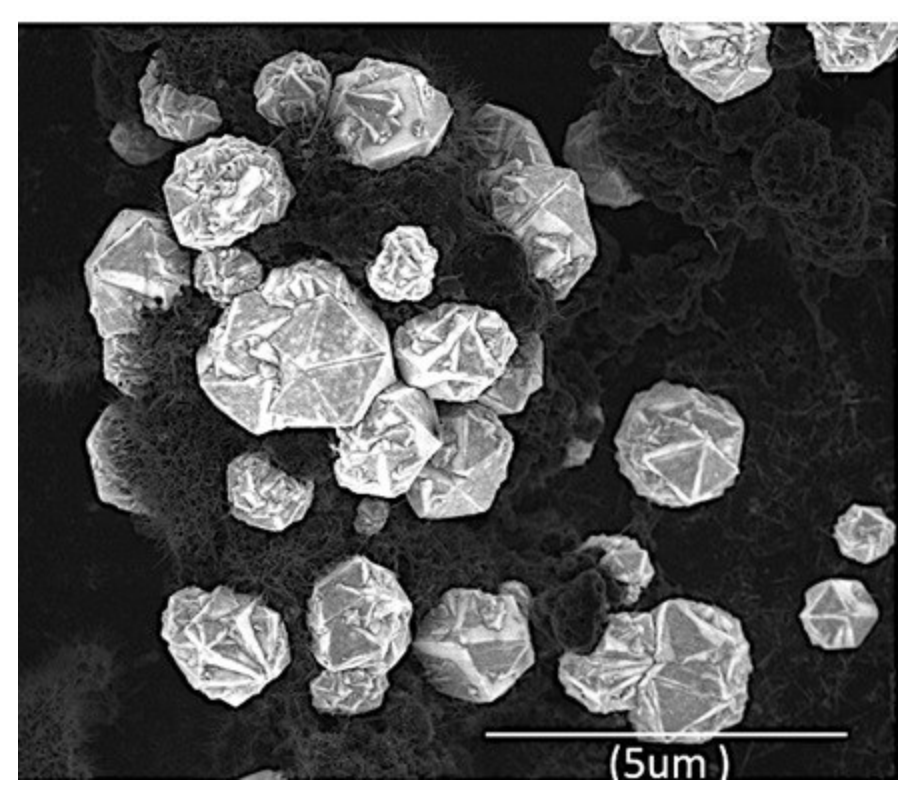
Jagdish Narayan, Roger J. Narayan: Methodology, Data curation, Writing- Original draft preparation, Writing- Reviewing and Editing.

## **Funding**

The authors also wish to acknowledge National Science Foundation grants 1836767, 2029974, and 2037636.

### **Competing Interests**

The authors declare that they have no known competing financial interests or personal relationships that could have appeared to influence the work reported in this paper.



**Graphical Abstract** 

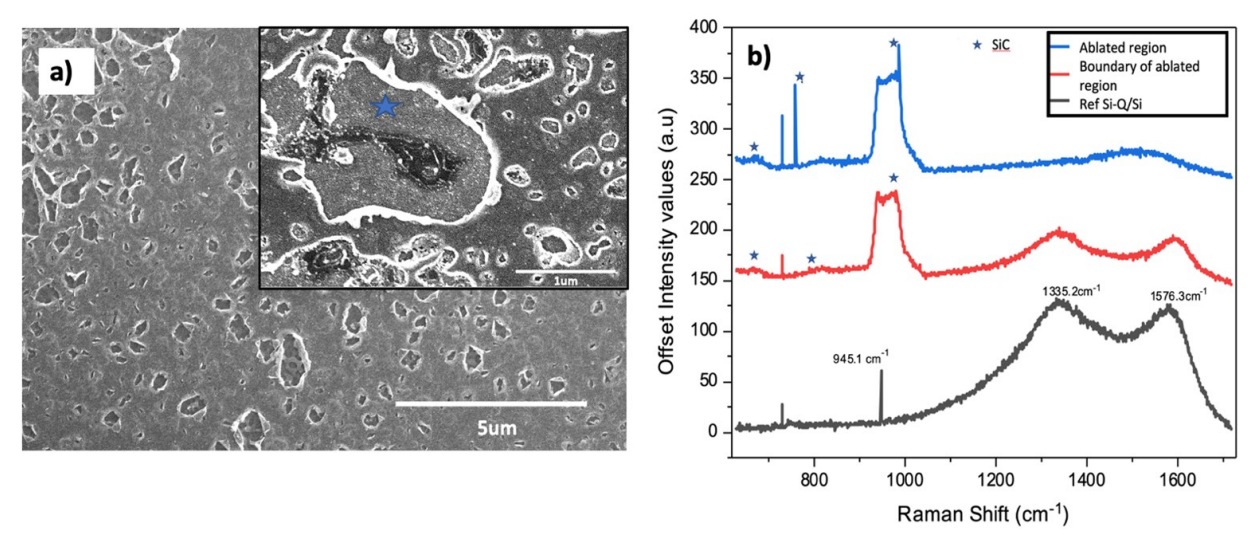


Figure 1

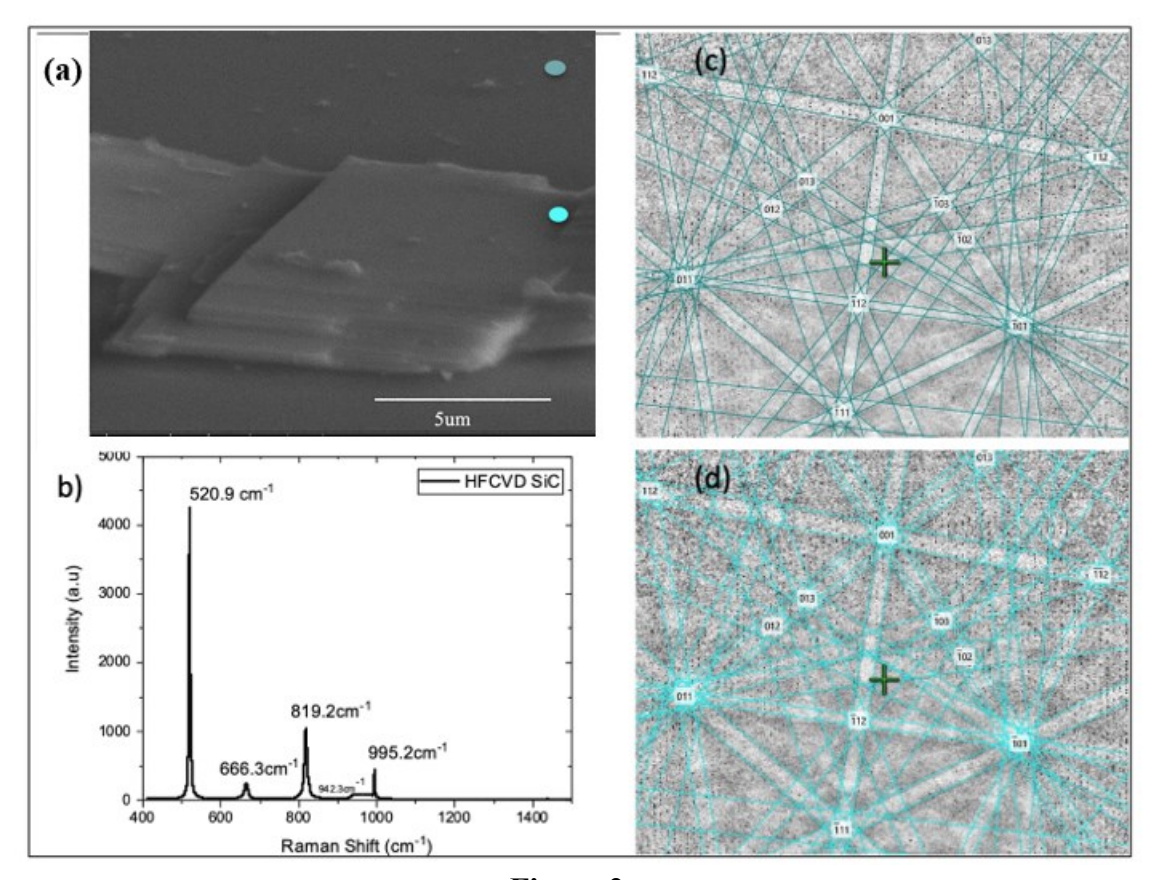


Figure 2

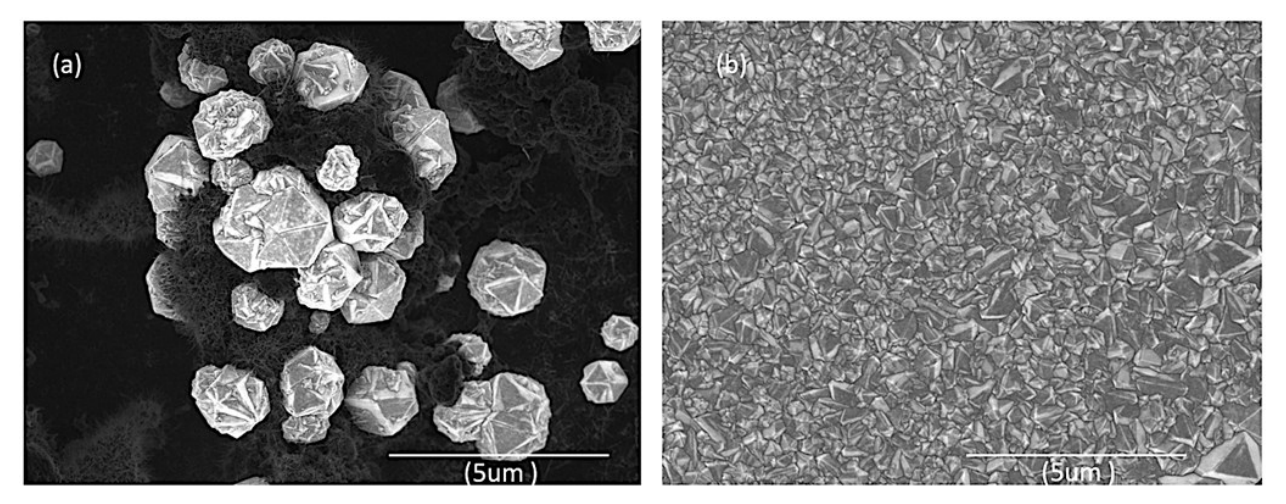


Figure 3

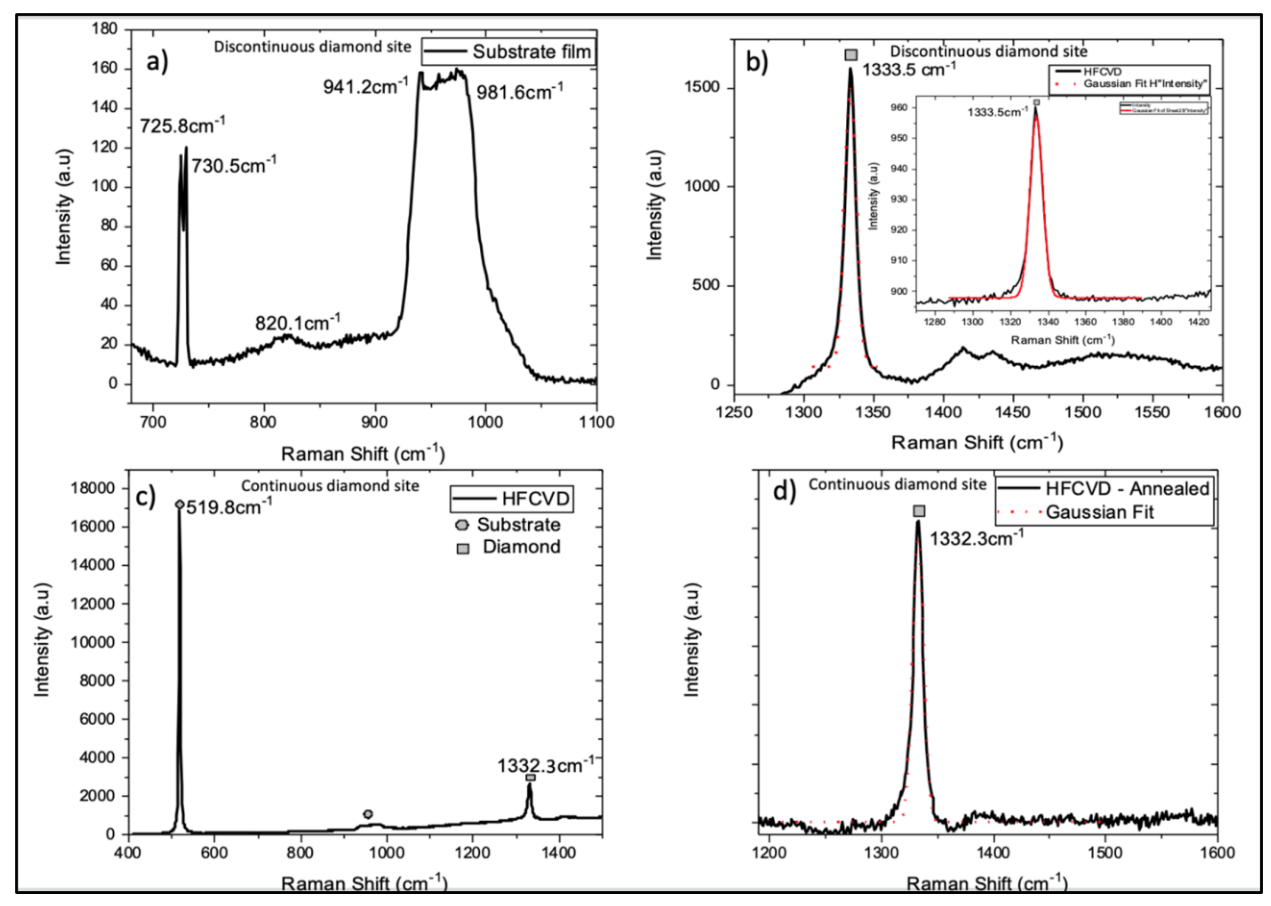


Figure 4

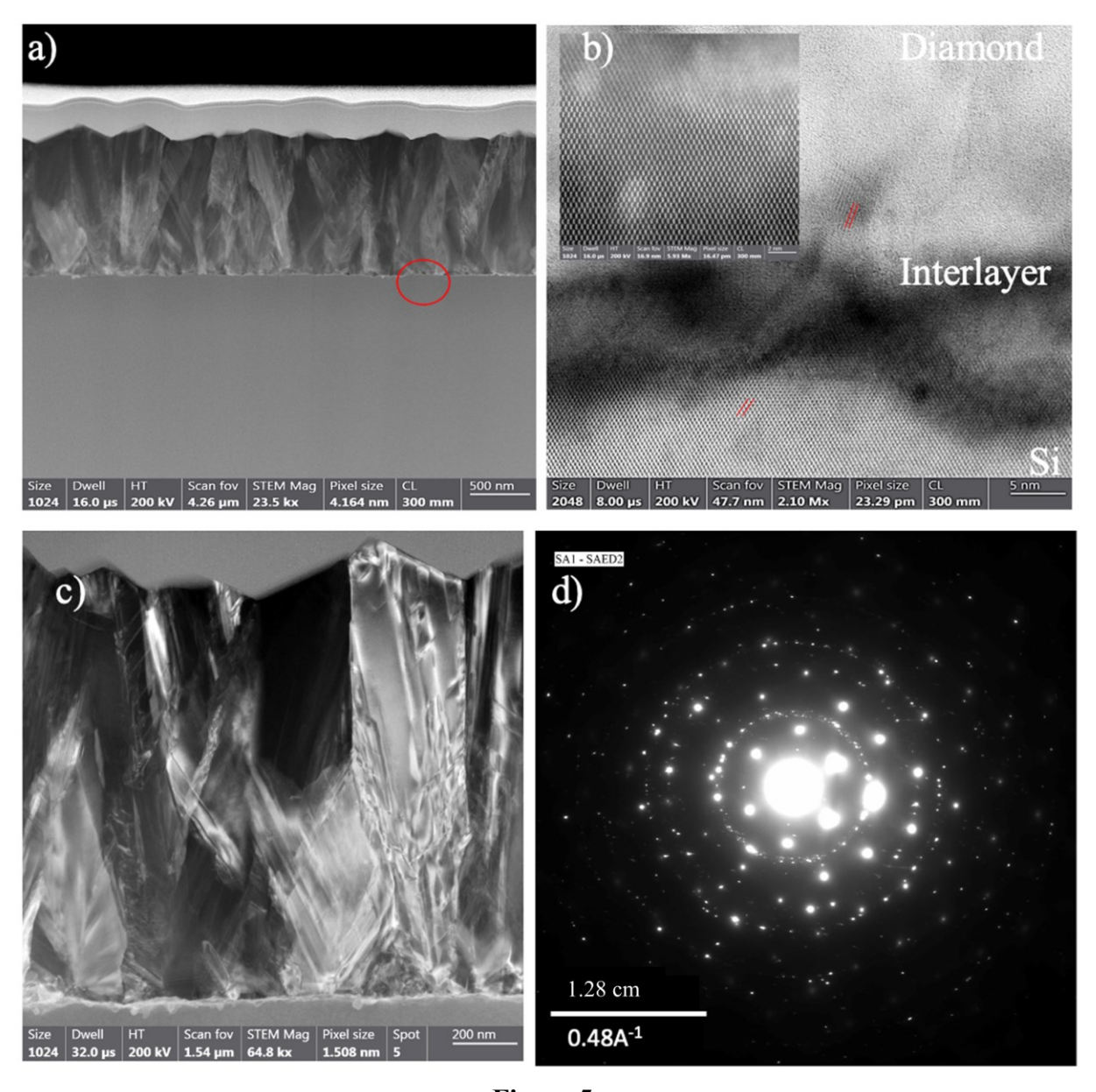


Figure 5

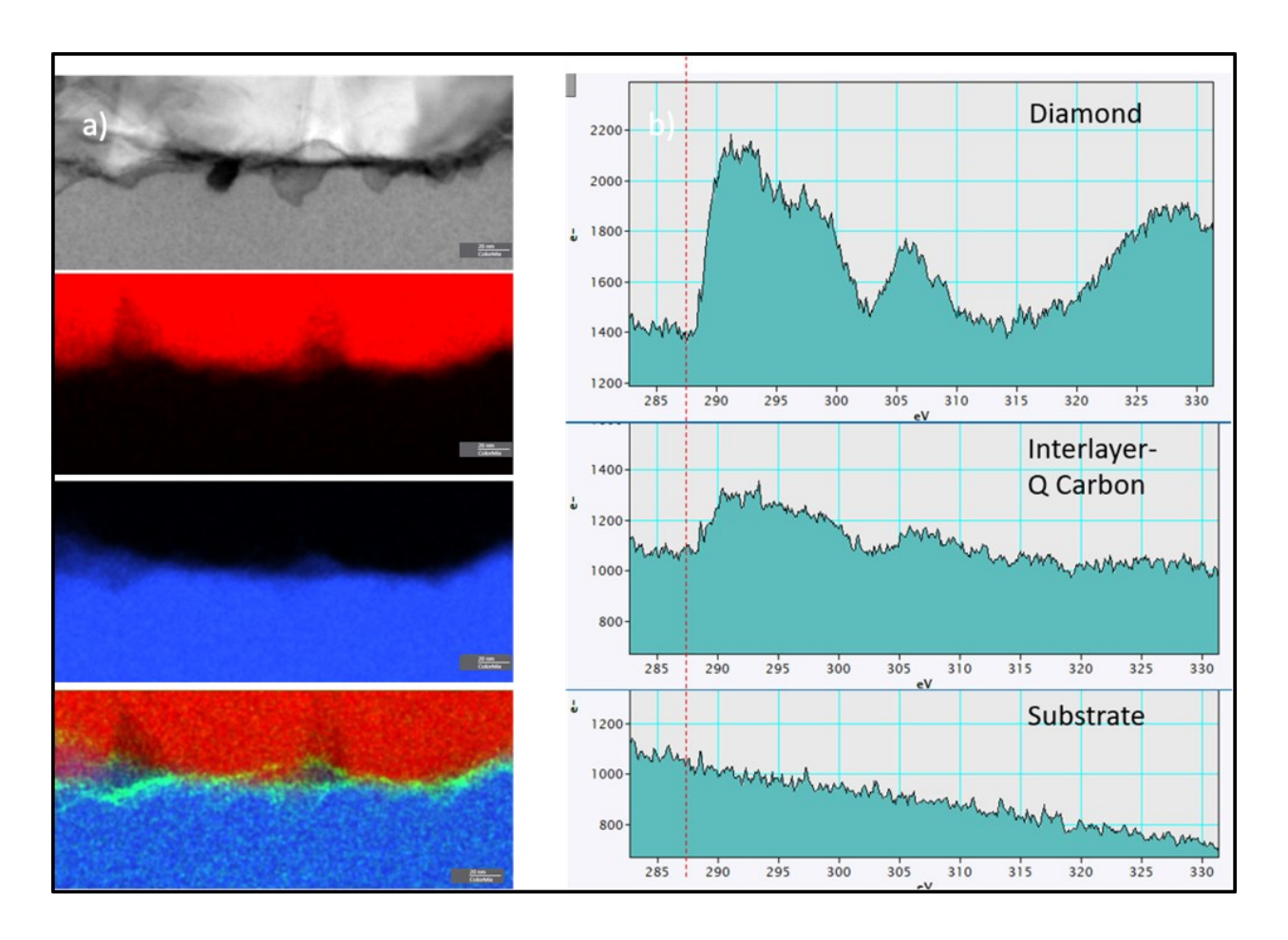


Figure 6

# **Figure Captions**

Figure 1(a). Surface image of Si-Q carbon film post annealing. The inset is at higher magnification showing the formation of nano-sized 3c-SiC (region in blue) which is circumscribed nanodiamonds, (b) Raman spectra showing evolution of 3c-SiC phase post laser annealing the Si-Q carbon on silicon.

- Figure 2. (a) SEM image showing the formation of plate structures of 6H-SiC on Si using Si-Q interlayer, (b) Raman spectrum at 6H-SiC plates, EBSD showing the kikuchi patterns at (c) Si, and (d) 6H-SiC.
- Figure 3. HRSEM images. (a) discontinuous diamond film growth on SiC interlayer having average size of 1.8  $\mu$ m. (b) high nucleation continuous diamond film on Q-Carbon interlayer on (100) Si..
- Figure 4. Raman spectra showing (a) presence of SiC at the site of discontinuous microdiamonds. (b) formation of microdiamonds nucleating on SiC with the inset showing Gaussian fitting. (c) formation of continuous microdiamonds without the presence of SiC. (d) Gaussian fitting of diamond nucleating continuously.
- Figure 5. High-resolution STEM and EELS from cross-sectional diamond on Q-carbon interlayer on Silicon sample using FEI titan. (a) Cross-sectional HRSTEM showing the platinum layer, diamond, interlayer and silicon substrate. (b) the <110> HRSTEM image showing individual column of atoms on diamond in some focused grains due to columnar grain structure, amorphous interlayer and silicon substrate, with inset of silicon. (c) HRSTEM image showing columnar growth structure of diamonds. (d) <110> diffraction pattern from diamond and silicon.
- Figure 6. (a) HDAAF image and Chemical mapping of the cross-section. (b) EELS spectrum from Carbon scan showing  $\pi^*$  (red line) and  $\sigma^*$  edges in the interlayer, and only  $\sigma^*$  edge in diamonds showing the presence of Q-carbon in the interlayer.